The Effect of Interfacial Mass Transfer on Steady-State Water Radiolysis

P. A. Yakabuskie, J. M. Joseph and J. C. Wren[1]
[1] University of Western Ontario, London, Ontario, Canada

Abstract

The effect of headspace on the γ-radiolysis of water was studied as a function of gas-to-liquid volume ratio at various solution pHs and cover gas compositions. Experimental results were compared with computer simulations using a water radiolysis kinetics model. The steady-state aqueous concentration of H_2 was found to be proportional to the product of the cover gas volume and gaseous H_2 concentration over the entire pH and cover-gas composition range studied. This result is important for predictions of hydrogen production rates during radiolysis of water and the resulting release of such hydrogen to gas volumes in reactor systems.

1. Introduction

Accurate understanding of the effects of ionizing radiation on nuclear reactor system chemistry and materials performance are important for assessment of various operational and maintenance requirements and safety margins of nuclear power plants. Of particular concern is the chemistry driven by the radiolysis of water. Deposition of ionizing radiation into water leads to the formation of primary water radiolysis products as given in R1:

$$H_2O \xrightarrow{rad} \bullet OH, \bullet e_{aq}^-, H\bullet, HO_2\bullet, H_2, H_2O_2, H^+ \qquad (R1)$$

The primary water decomposition products differ considerably in their chemical reactivity and redox property. They can participate in electrochemical reactions leading to corrosion, and understanding their production rates and subsequent reactions can provide the basis for selecting materials and water chemistry control agents to mitigate corrosion.

The most studied parameter for radiolysis of a solution (typically water with an additive) has been the primary radiolysis yields, often expressed using G-values in units of number of species formed per 100 eV of absorbed energy. These are the product yields when the products reach homogeneous distribution along the radiation track, and are typically obtained in a 10 to 100 ns time scale following deposition of finite (short term) pulse radiation energy. The primary radiolysis products, once generated, undergo further chemical reactions with each other, water molecules and any other chemical species in solution, and the solution chemistry changes with time. The reactions of the primary radiolysis products in this longer term stage can be treated as bulk-phase processes, and the changes can be described using classical chemical reaction rate and transport equations and using macroscopic properties such as concentration, temperature, or thermodynamic state properties of the solution.

The elementary reactions of the primary radiolysis products with each other and other water-derived species have been studied extensively [1-4]. Pulse radiolysis studies have been extremely useful for establishing the primary radiolysis yields and the rates of fast free radical and ion reactions [5]. With a constant (or slowly changing) radiation source, radiation energy deposition is continuous, and the solution chemistry evolves towards a steady state in which the concentrations of radiolysis products differ substantially from the concentrations associated with the primary radiolysis yields or the final molecular products. The bulk phase chemical reaction rates are very sensitive to aqueous environments such as pH, temperature and chemical additives that, in particular, can be involved in acid-base equilibrium and redox reactions. Thus, while changes in aqueous environment such as pH or the presence of chemical additives at low concentrations will not significantly affect the primary radiolysis yields, they can significantly influence the subsequent chemical reactions, altering the eventual steady-state species concentrations. For example, the concentrations of H_2 and H_2O_2 are more than two orders of magnitude greater in water with a pH of 10.6 compared to water with a pH of 6.0 following an extended period of γ-radiolysis, yet the primary yields for these species remain constant over this same pH range [6].

For most situations of practical interest, radiation fields are present on a continuous basis. Most corrosion processes, or other processes involving interfacial transport, have high activation energies and only occur substantially over long time periods. Hence, constant radiation fields will drive water radiolysis chemistry that can influence the corrosion of reactor structural materials over those time scales. To assess the impact of long-term radiolysis on corrosion requires that we understand and can predict the speciation and concentrations in water under steady-state conditions, and particularly in the presence of species that are used for redox chemistry control in nuclear systems.

Water radiolysis produces two volatile species, H_2 and O_2. In the presence of a headspace or cover gas volume, these species can transfer to the gas phase until equilibrium is established (or O_2 may transfer from the gas phase to the liquid phase when air is introduced into a cover gas). The impact of this aqueous-gas interfacial mass transfer on radiolysis driven chemistry has not been studied systematically. This is important because it can impact on predictions of hydrogen gas generation, particularly if the headspace communicates with other gas volumes. Volumes of hydrogen in the gas phase are important because they represent a potential combustion hazard. Interfacial transfer of volatile species can also alter the aqueous phase concentrations, and because of the complex chemistry, affect the steady-state concentrations of the reactive species that are most important in controlling corrosion rates. Quantitative understanding of interfacial mass transfer and its connection to the aqueous state has another important application. Measurement of the amount of H_2 and O_2 in a gas sample is much simpler and more accurate than measurement of the quantities of these species dissolved in water. Under many extreme experimental conditions, as with in-plant system chemistry monitoring, cover-gas analysis may be the only practical measurement that can be carried out.

This study examines the effect of interfacial transfer of the volatile radiolysis products H_2 and O_2 on steady-state water radiolysis chemistry by performing experiments and analyzing their results using a water radiolysis chemical kinetics model that includes the aqueous-gas phase transfer kinetics of the volatile species.

2. Experimental

All experiments were performed with water purified to a resistivity of 18.2 MΩ·cm using a NANOpure Diamond UV ultrapure water system from Barnstead International. The experiments at pH 6.0 were performed without the addition of any buffer and those performed at pH 10.6 used a phosphate buffer (10^{-3} mol·dm^{-3}). The pH of the solution was measured prior to, and at the end of, the irradiation period using an Accumet pH meter. The samples were irradiated in 20 mL glass vials that were capped using aluminum crimp caps with PTFE silicone septa (Agilent Technologies) to provide a vacuum tight seal so as to ensure no loss of gaseous species. The de-oxygenated water samples were prepared by purging a bulk solution with ultra high purity argon (impurity < 0.001%), for more than one hour. The solution was then transferred into glass vials sealed inside an Ar-purged glove box where the oxygen concentration was maintained below 1000 ppm. For aerated samples, a bulk solution was saturated with hydrocarbon free air (Praxair) for more than one hour and individual vials were saturated for 10 minutes and capped, before the solution was transferred into the vials with a syringe. The experiments were performed with different ratios of gas volume to aqueous volume, V_g/V_{aq}, in the vials with the aqueous-gas interfacial area held constant at 3.14 cm^2 (the cross-sectional area of the vials).

Irradiation was carried out in a ^{60}Co gamma cell (MDS Nordion) which provided the irradiation chamber with a uniform absorption dose rate of 2.5 Gy·s^{-1} determined using Fricke dosimetry [4,7]. The vials were held in a specially designed sample holder so as to have a reproducible uniform dose distribution during irradiation. Individual vials were taken out of the gamma cell at regular time intervals and the gas and liquid phases were sampled and analyzed for H_2 and H_2O_2, respectively.

The concentration of hydrogen peroxide was determined by the Ghormley tri-iodide method in which I^- is oxidized to I_3^- by H_2O_2 in the presence of ammonium molybdate catalyst [8]. The I_3^- concentration was measured using UV spectrophotometry of the I_3^- absorption at 350 nm with a molar extinction coefficient of 25500 $M^{-1}\cdot cm^{-1}$ [9]. Using this method, the detection limit for $[H_2O_2]$ was 3×10^{-6} mol·dm^{-3} and the uncertainties in the measurement arising from sampling and instrumental errors were estimated to be ±0.2% at the lower end of the measured concentration range and ±0.05% at the higher end of the measured range. The H_2O_2 analysis was performed immediately after removal of a vial from the gamma cell to minimize any thermal decomposition of H_2O_2 in the sample vials.

The gas sampling was carried out using a gas-tight syringe with a luer lock valve (Agilent Technologies) and gas samples were injected into the GC through a gas-sampling valve and septum into the sample loop. The GS-GASPRO column used is connected to three detectors; Thermal Conductivity Detector (TCD), μ-Electron Capture Detector (μ-ECD) and Mass Selective Detector (MSD). Quantification of the amount of H_2 in the cover gas was performed using the TCD detector and nitrogen is used as the carrier gas at a flow rate of 4.6 ml/min. Using this method, the detection limit for the gaseous concentration $[H_2(g)]$ was 1.0×10^{-5} mol·dm^{-3} and the uncertainties in the measurement arising from sampling and instrumental errors were estimated to be ±50 % at the low end of the measured concentration range and ±0.005 % at the high end of the concentration range.

3. Interfacial mass transfer in the radiolysis model

3.1 Radiolysis kinetic model for pure water phase

We have assembled a radiolysis reaction kinetics model for pure liquid water consisting of about 40 elementary homogeneous reactions with well-defined rate constants, including primary radiolysis production, subsequent reactions of the radiolysis products with each other, hydrolysis reactions and the related acid-base equilibria. This model, described in detail elsewhere [6], has been shown to reproduce the steady-state radiolysis data of liquid water observed under a wide range of conditions [6,10,11]. This reaction kinetics model, with additional 'reactions' to address the aqueous-gas phase transfer of H_2 and O_2, is used in the analysis of the experiments reported here.

3.2 Aqueous-gas interfacial transfer

To address the interfacial transfer of H_2 and O_2, two phase equilibria are included in our standard radiolysis model:

$$H_2(aq) \leftrightarrows H_2(g) \quad \text{(R2)}$$

$$O_2(aq) \leftrightarrows O_2(g) \quad \text{(R3)}$$

where $H_2(g)$ and $O_2(g)$ represent H_2 and O_2 in the gas phase. The designation of (aq) and (g) is used only for H_2 and O_2 in the following kinetics discussion because all other species associated with pure water radiolysis have negligible volatility and will remain in the aqueous phase throughout the experiments.

The interfacial mass transfer kinetics is modeled based on the assumption that the transfer rate depends on a driving force (usually a concentration differential from that of equilibrium) and a resistance represented by an overall interfacial transfer coefficient, υ_{int}^{i} of species i:

$$\frac{dC_{aq}^{i}(t)}{dt} = -\frac{V_g}{V_{aq}}\frac{dC_g^{i}(t)}{dt} = -\upsilon_{int}^{i}\cdot\frac{A_{int}}{V_{aq}}\cdot\left(1-K_p^{i}\cdot\frac{C_g^{i}(t)}{C_{aq}^{i}(t)}\right)\cdot C_{aq}^{i}(t) \quad \text{(Eq. 1)}$$

where $C_{aq}^{i}(t)$ and $C_g^{i}(t)$ are the aqueous and gas phase concentrations of species *i* at time t, A_{int} is the gas/aqueous phase interfacial area, and V_{aq} and V_g are the aqueous and gas phase volumes, respectively. The partition coefficient, K_p^{i}, is one form of Henry's constant and is defined as the ratio of aqueous and gas phase concentrations of species *i* at phase equilibrium:

$$K_p^{i} = \frac{C_{aq}^{i}(eq)}{C_g^{i}(eq)} \quad \text{(Eq. 2)}$$

The interfacial mass transfer equation can be rewritten in the form of a first order reaction as

$$\frac{dC_{aq}^{i}(t)}{dt} = -\frac{V_g}{V_{aq}}\frac{dC_g^{i}(t)}{dt} = -k_{app}^{i}(t)\cdot C_{aq}^{i}(t) \quad \text{(Eq. 3)}$$

by defining a net mass transfer coefficient that is time dependent, $k_{app}^{i}(t)$:

$$k_{app}^{i}(t) = \upsilon_{int}^{i} \cdot \frac{A_{int}}{V_{aq}} \cdot \left(1 - K_{p}^{i} \cdot \frac{C_{g}^{i}(t)}{C_{aq}^{i}(t)}\right) \qquad \text{(Eq. 4)}$$

These transport rate equations are incorporated in our model of rate equations for radiolysis reactions.

The radiolysis model does not contain any reactions associated with the radiolysis of water vapour in the headspace. The density of water molecules in the gas phase at room temperature is low compared to liquid water phase and this justifies this neglect. Our ability to model the observed chemistry over a wide range of conditions supports this approximation for our test conditions.

4. Results and discussion

4.1 General observations

The concentrations of H_2 in the headspace, $[H_2(g)]$, were measured for samples at pH 6.0 and pH 10.6 under aerated and deaerated conditions. For these experiments the gas-to-aqueous volume ratio, V_g/V_{aq}, was 1:1. Under all conditions, $[H_2(g)]$ increases linearly with time except early times. Since the only source of $H_2(g)$ is the aqueous to gas phase transfer of $H_2(aq)$ that is radiolytically produced, the linear increase in $[H_2(g)]$ with time suggests that $[H_2(aq)]$ quickly reaches steady state. The different slopes further suggest that different steady-state concentrations of $H_2(aq)$ are reached under different conditions. The previous experimental and model simulation study on γ-radiolysis has shown that in the absence of headspace, $[H_2(aq)]_{SS}$ varies from 1.8×10^{-6} mol·dm^{-3} (below detection limit) to 2.0×10^{-5} (2.6×10^{-5}), 4.1×10^{-4} (2.0×10^{-4}) and 5.3×10^{-4} (1.9×10^{-4}) mol·dm^{-3} as the condition changes from pH 6.0/deaerated, to pH 6.0/aerated, pH 10.6/deaerated, and pH 10.6/aerated, where the values are model predictions and the measured concentrations are in brackets [6].

The effect of aqueous-gas phase partitioning on water radiolysis chemistry was studied in detail under pH 6.0/aerated and pH 10.6/deaerated conditions by varying the gas-to-aqueous volume ratio from 4:1 to 1:4. The time-dependent concentrations of H_2 in the headspace, $[H_2(g)]$, and H_2O_2 in the aqueous phase, $[H_2O_2]$, observed as a function of V_g/V_{aq} are presented in Figure 1 for aerated water at pH 6.0 and in Figure 2 for deaerated water at pH 10.6. The model predictions are shown as solid lines. For aerated water at pH 6.0, after a short delay $[H_2(g)]$ increases linearly with irradiation time and the rate of the increase is inversely proportional to V_g, while H_2O_2 quickly reaches a steady-state concentration, $[H_2O_2]_{SS}$, that is nearly independent of V_g or V_{aq}. For deaerated water at pH 10.6, a similar trend is observed for $[H_2(g)]$, but the time dependent behaviour of $[H_2O_2]$ is different. The $[H_2O_2]$ continuously increases with time, and does not reach a steady-state level within the 5 h experimental period. Also, the rate of increase in $[H_2O_2]$ is progressively slower with increasing V_g/V_{aq} ratio. These observations indicate that $[H_2(g)]$ does not have a simple dependence on $[H_2O_2]$ or possibly the concentrations of other radiolytically produced species.

One important implication of this observation is that the measurement of $[H_2(g)]$ alone is not sufficient to determine the water radiolysis chemistry.

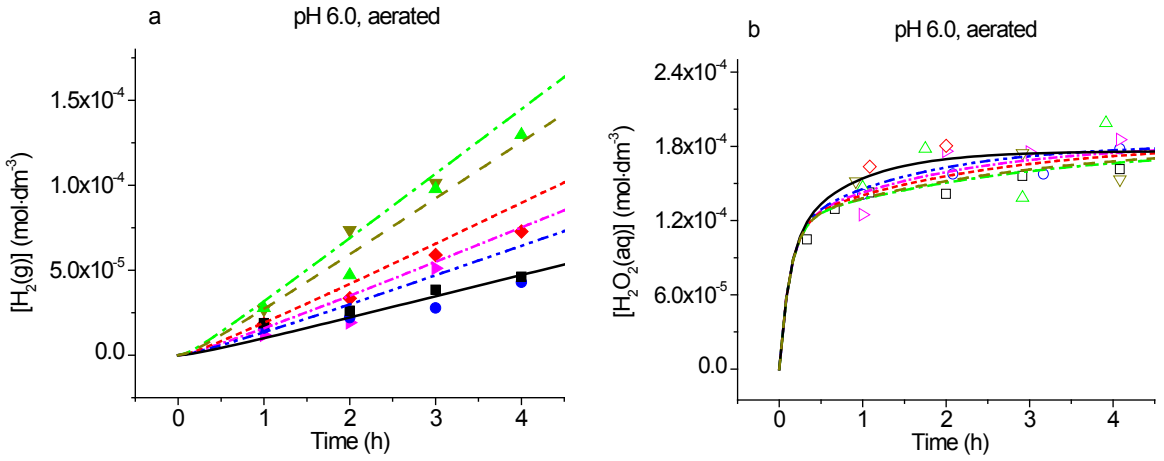

Figure 1: H_2 concentrations in the headspace (a) and H_2O_2 concentrations in the aqueous phase (b) as a function of irradiation time for aerated water at pH 6.0 at 2.5 $Gy \cdot s^{-1}$. The symbols represent the experimental data and the lines the radiolysis model results. The H_2 data are shown with solid symbols and H_2O_2 with open symbols for different V_g:V_{aq} ratios; Respectively,

4:1 (■,□,—), 3:2 (●,○,–··), 1:1 (▶,▷,-·-), 2:3 (◆,◇,---), 1:3 (▼,▽,——) and 1:4 (▲, △ , –·–).

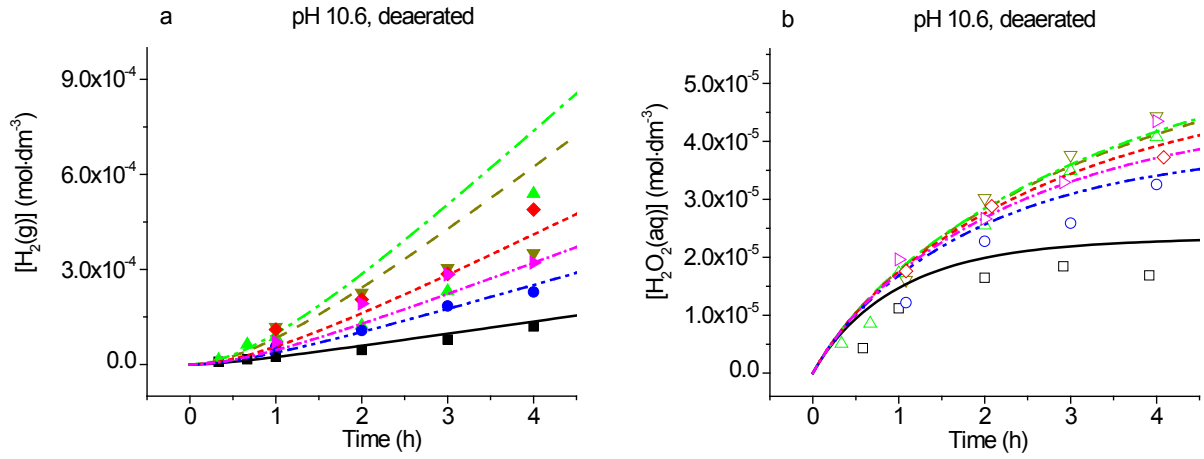

Figure 2: H_2 concentrations in the headspace (a) and H_2O_2 concentrations in the aqueous phase (b) as a function of irradiation time for deaerated water at pH 10.6 at 2.5 $Gy \cdot s^{-1}$. The symbols represent the experimental data and the lines the radiolysis model results. The H_2 data are shown with solid symbols and H_2O_2 with open symbols for different V_g:V_{aq} ratios; Respectively,

4:1 (■,□,—), 3:2 (●,○,–··), 1:1 (▶,▷,-·-), 2:3 (◆,◇,---), 1:3 (▼,▽,——) and 1:4 (▲, △ , –·–).

The model described in Section 3 reproduces the experimental results for both $[H_2(g)]$ and $[H_2O_2]$ within experimental uncertainties. In a previous study, we have shown that the same

radiolysis kinetics model reproduces the radiolysis behaviour of pure water without a cover gas under a wider range of conditions [6]. The ability of the model with interfacial transport kinetics to match our experimental observations further confirms that the kinetics model includes all of the necessary elementary reactions for prediction of continuous radiolysis of water. Sensitivity and parametric analyses were carried out to determine the main mechanism by which the interfacial transfer of H_2 and O_2 affects the aqueous phase reactions during continuous radiolysis.

4.2 Radiolytic production of H_2(g) in the cover gas

The source of H_2 in the cover gas is the aqueous-to-gas phase transfer of hydrogen produced in the aqueous phase, H_2(aq), by radiolytic decomposition of liquid water:

$$H_2(aq) \quad \rightarrow \quad H_2(g) \qquad\qquad k_{app}^{H_2}(t) \qquad\qquad \text{(R4)}$$

where the net interfacial transfer rate constant, $k_{app}^{H_2}(t)$, defined in Eq. 3 and Eq. 4, decreases with time as the system approaches the equilibrium concentrations of H_2 in the two phases. At phase equilibrium, $k_{app}^{H_2}(t)$ is zero, and the gas- and aqueous-phase concentrations of H_2 are determined by the phase equilibrium partition coefficient, see Eq. 2. The partition coefficient of H_2, $K_P^{H_2}$, as defined in Eq. 2, is 0.019 at 25ºC and smaller at higher temperatures. In a constant radiation field there will be continuous radiolytic production of H_2. For a highly volatile gas like H_2, if its initial concentration in the gas phase is negligible, the system will remain far away from phase equilibrium even over a long period of irradiation. During the early time after start of irradiation, $t << t_{\text{int}}^{eq}$, it can be assumed that

$$k_{app}^{H_2}(t) \approx k_{app}^{H_2}(t=0) = \upsilon_{\text{int}}^{H_2} \cdot \frac{A_{\text{int}}}{V_{aq}} \qquad \text{(Eq. 5)}$$

From Eq. 3, the rate of change in the concentration of H_2(g) under this condition is

$$\frac{d}{dt}\left[H_2(g)\right]_t^{HS} \approx \upsilon_{int}^{H_2} \cdot \frac{A_{int}}{V_g} \cdot \left[H_2(aq)\right]_t^{HS} \qquad \text{(Eq. 6)}$$

This equation predicts that for an interfacial geometry defined by V_{aq}, V_g and $A_{int,}$ the rate of H_2(g) production is proportional to $\left[H_2(aq)\right]_t^{HS}$. Thus, if the concentration of H_2(aq) does not change significantly with time, i.e., if the aqueous system reaches (pseudo-) steady state relatively quickly, $\left[H_2(g)\right]_t^{HS}$ will increase linearly with irradiation time:

$$\left[H_2(g)\right]_t^{HS} \approx \upsilon_{\text{int}}^{H_2} \cdot \frac{A_{\text{int}}}{V_g} \cdot \left[H_2(aq)\right]_{SS}^{HS} \cdot (t - t_{ss}) + \left[H_2(g)\right]_{t_0}^{HS} \qquad \text{(Eq. 7)}$$

where $\left[H_2(aq)\right]_{SS}^{HS}$ represents the steady-state concentration of H_2(aq), t_{SS} the time to establish steady state in the aqueous system, and $\left[H_2(g)\right]_{t_0}^{HS}$ the concentration of H_2(g) in the gas phase

at t_0. This linear increase in $[H_2(g)]_t^{HS}$ is observed at both pHs as shown in Figures 1a and 2a. The linear increase region is established more slowly at pH 10.6 than at pH 6.0 and this is attributed to the longer time required for H_2(aq) to reach steady state at pH 10.6 [6].

The most important aspect of Eq. 6 is that it predicts the rate of increase in the gaseous concentration of H_2(g) in the gas phase is proportional to $[H_2(aq)]_t^{HS}$. This relationship is difficult to confirm experimentally because it is difficult to measure the aqueous concentration of H_2(aq) with a reasonable accuracy. Measurements of $[H_2(aq)]_t^{NHS}$ in tests without a headspace cannot be used to determine $[H_2(aq)]_t^{HS}$ because the transfer of H_2 to the gas phase can influence $[H_2(aq)]_t^{HS}$.

The dissolved H_2 concentration, $[H_2(aq)]_t^{HS}$, and aqueous H_2O_2 concentration, $[H_2O_2(aq)]_t^{HS}$, were modeled for the different ratios of gas and liquid volumes (V_g/V_{aq}), as well as for no headspace present. For H_2O_2, experimental data was also collected for each volume ratio, and agreed with the model simulation within experimental uncertainties. The model calculations predict that the presence or absence of headspace on $[H_2(aq)]_t^{HS}$ is negligible at pH 6.0. However, at pH 10.6 it is no longer negligible and $[H_2(aq)]_t^{HS}$ depends on the available gas volume. The behaviour of $[H_2O_2(aq)]_t^{HS}$ exhibits a similar pH dependence to that of $[H_2(aq)]_t^{HS}$, indicating that the behaviour of other radiolysis products in the aqueous phase can be inferred from that of H_2O_2 which can be more easily measured experimentally. The small difference in the influence of a headspace on $[H_2(aq)]_t^{HS}$ versus $[H_2O_2(aq)]_t^{HS}$ arises from the fact that $[H_2(aq)]_t^{HS}$ is affected by the interfacial transfer of H_2 while $[H_2O_2(aq)]_t^{HS}$ is affected by the transfer of O_2 as well as H_2.

To analyze the data we rearrange Eq. 6 as

$$log\left(V_g \cdot \frac{d[H_2(g)]_t^{HS}}{dt}\right) \approx log\left(\upsilon_{int}^{H_2} \cdot A_{int}\right) + log[H_2(aq)]_t^{HS} \qquad \text{(Eq. 8)}$$

In Figure 3, the $d[H_2(g)]_t^{HS}/dt$ values, obtained from the slopes of the linear regions of the $[H_2(g)]_t^{HS}$ vs time plots in Figures 1a and 2a and multiplied by the cover gas volume, are plotted against the calculated (pseudo) steady-state concentrations, $[H_2(aq)]_{SS}^{HS}$. In Figure 3, the data are shown in a log-log plot due to the large span in $[H_2(aq)]_{SS}^{HS}$. A linear fit to the log-log data in Figure 3 has a slope of 1.000 and an intercept $\log\left(\upsilon_{int}^{H_2} \cdot A_{int}\right)$ of -2, confirming that Eq. 6 and Eq. 8 hold under all conditions. This result confirms that the concentration of H_2 in the liquid water phase during irradiation can be derived from the more easily measurable mass of H_2(g) (= V_g × the gaseous concentration of H_2(g)) in the headspace, irrespective of conditions of the irradiation.

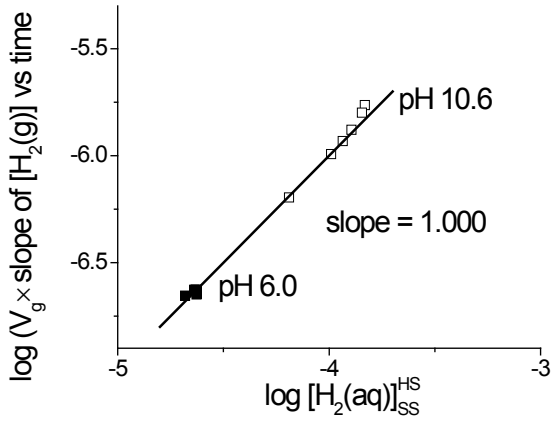

Figure 3: The log of (Vg × slope of $[H_2(g)]$ vs time) is shown as a function of $\log\left[H_2(aq)\right]_{SS}^{HS}$ for aerated water at pH 6.0 and deaerated water at pH 10.6.

The results of this work, as shown in Figures 1 and 2, demonstrate that the presence of headspace will have an impact on the concentrations of radiolytically produced aqueous species, and this influence depends on pH. The work reported here has been conducted at only two pH values because these are sufficient to sample two different regions for water radiolysis chemistry. Our previous study on water radiolysis in the absence of a headspace has established that the kinetic behaviour of the water decomposition products and their consequential steady-state concentrations can vary considerably over the pH range of $8 < pH < 11$, whereas outside this range they are nearly independent of pH [6].

5. Conclusions

In many real environments where radiolysis of water can occur, a connecting gas volume is present. This study has examined the impact of such a cover gas on the water chemistry driven by radiolysis. We have studied the effect of the aqueous-gas phase interfacial transfer of volatile species, H_2 and O_2, on steady-state radiolysis chemistry. At pH ≤ 8, the effect of aqueous-to-gas phase transfer of these volatile species on the concentrations of the other aqueous species generated by radiolysis is negligible. Our experimental results confirm the capability of our chemical kinetics model, which predicts these results. For low pHs, the gaseous concentration of H_2 in a cover gas volume increases linearly with time during steady-state irradiation and the rate of increase is proportional to $1/V_g$, while the aqueous concentrations of $H_2(aq)$ and H_2O_2 are effectively independent of A_{int}/V_{aq}.

At higher pHs (≥ 8), radiolytic production of $O_2(aq)$ is slow but considerable. Thus, even without a headspace, the aqueous concentration of $H_2(aq)$ and H_2O_2 reach steady state more slowly and reach higher concentrations than those achieved for irradiation of water at lower pHs. In the presence of a headspace, the interfacial transfers of both H_2 and O_2 from the gas phase decrease the aqueous concentrations of the volatile species and indirectly alter the concentrations of H_2 and O_2 in solution by influencing the concentrations of radical species that control their concentrations. As a result, the aqueous concentration of $H_2(aq)$ is no longer independent of A_{int}/V_{aq}. Irrespective of the pH dependence a headspace implements on

system chemistry, the accumulated mass of $H_2(g)$ in the headspace (or $V_g \times [H_2(g)]$) is proportional to the aqueous concentration of $H_2(aq)$:

$$V_g \cdot [H_2(g)]_t^{HS} \approx \left(\upsilon_{int}^{H_2} \cdot A_{int} \cdot [H_2(aq)]_t^{HS}\right) \cdot t$$

Thus, the measurement of gaseous concentration of H_2 in the headspace can be used to infer the aqueous concentration of $H_2(aq)$.

The aqueous-gas phase transfer of radiolytically produced O_2 affects the concentrations of H_2O_2 more than $H_2(aq)$. Thus, the measurement of $[H_2(g)]$ alone is not sufficient to determine water radiolysis chemistry. Experiments and kinetic modeling have shown that measurements of $[H_2O_2]$ in solution in combination with measurement of $[H_2(g)]$ in the cover gas can be used in determining the concentrations of other radiolysis products that determine water chemistry under continuous irradiation conditions.

6. Acknowledgements

The work described herein was funded under the NSERC (Natural Science and Engineering Research Council of Canada) and AECL (Atomic Energy of Canada Limited) Industrial Research Chair Program on Radiation Induced Processes in Nuclear Reactor Environments. Canada Foundation for Innovation is greatly acknowledged for the grant for all of the instruments used in this study. The authors would like to acknowledge Drs. C. Stuart and D. Wren at AECL for their helpful discussion and the review of this work.

7. References

[1] Allen, A.O. “The Radiation Chemistry of Water and Aqueous Solutions”, Van Nostrand, New York, 1961.

[2] Draganic, I.G., Draganic, Z.D. “The Radiation Chemistry of Water”, Academic Press, New York, 1971.

[3] Farhataziz., Rodgers, M.A.J. “Radiation Chemistry: Principles and Applications”, VCH Publishers, New York, 1987.

[4] Spinks, J.W.T., Woods, R. J. “An Introduction to Radiation Chemistry”, Wiley, New York, 1990.

[5] Buxton, G.V., Greenstock, C.L., Helman, W.P., Ross, A.B. “Critical review of rate constants for reactions of hydrated electron, hydrogen atoms and hydroxyl radicals (•OH/•O^-) in aqueous solution”, J. Phys. Chem. Ref. Data., 17, 1988, pp.513-886.

[6] Joseph, J.M., Chio, B.S., Yakabuskie, P., Wren, J.C. “A combined experimental and model analysis on the effect of pH and $O_2(aq)$ on γ-radiolytically produced H_2 and H_2O_2”, Radiat. Phys. Chem. 77(9), 2008, pp. 1009-1020.

[7] Upadhyay, S.N., Ray, N.K., Goel, H.C. “Dose distribution inside gamma cell 5000”, Indian J. Nucl. Med. 17(1), 2002, pp.35-41.

[8] Hochanadel, C.J. “Effect of cobalt gamma-radiation on water and aqueous solutions”, J. Phys. Chem. 56, 1952, pp.587-594.

[9] Stefanic, I., LaVerne, J.A. “Temperature dependence of the hydrogen peroxide production in the gamma-radiolysis of water”, J. Phys. Chem. A. 106(2), 2002, pp.447-452.

[10] Wren, J.C., Ball, J.M. “LIRIC 3.2 An updated model for iodine behaviour in the presence of organic impurities”, Radiat. Phys. Chem. 60(6), 2001, pp.577-596.

[11] Wren, J.C., Glowa, G.A. “A simplified kinetic model for the degradation of 2-butanone in aerated aqueous solutions under steady state gamma-radiolysis”, Radiat. Phys. Chem. 58(4), 2000, pp.341-356.